CO_2 hydrogenation to methanol over catalysts derived from single cationic layer CuZnGa LDH precursors

Molly M.-J. Li[1], Chunping Chen[2], Tuğçe Ayvalı[1], Hongri Suo[1,2], Jianwei Zheng[1], Ivo F. Teixeira[1], Lin Ye[1], Hanbo Zou[1], Dermot O'Hare[2], Shik Chi Edman Tsang[1]*

[1] Wolfson Catalysis Centre, Department of Chemistry, University of Oxford, Oxford, OX1 3QR, UK

[2] Chemistry Research Laboratory, University of Oxford, 12 Mansfield Road, Oxford, OX1 3TA, UK

* Corresponding author: edman.tsang@chem.ox.ac.uk

ABSTRACT:

Ultra-thin (1–3 cationic-layers) $(CuZn)_{1-x}Ga_x$-CO_3 layered double hydroxides (LDH) nanosheets were synthesized following the aqueous miscible organic solvent treatment (AMOST) method and applied as catalyst precursors for methanol production from CO_2 hydrogenation. It is found that upon reduction, the aqueous miscible organic solvent treated LDH (AMO-LDH) samples above a critical Ga^{3+} composition give consistently and significantly higher Cu surface areas and dispersions than the catalysts prepared from conventional hydroxyl-carbonate phases. Owing to the distinctive local steric and electrostatic stabilization of the ultra-thin LDH structure, the newly formed active Cu(Zn) metal atoms can be stably embedded in the cationic layers, exerting an enhancement to the catalytic reaction. The best catalyst in this study displayed methanol productivity with a space-time yield of 0.6 $g_{MeOH}{\cdot}g_{cat}^{-1}{\cdot}h^{-1}$ under typical reaction conditions, which as far as we are aware, is higher than most reported Cu-based catalysts in the literature.

Keywords: Cu/Zn/Ga catalysts, metal nanoparticle, layered double hydroxides, methanol synthesis, CO_2 hydrogenation.

Introduction

Cu/ZnO based catalysts are well known to be active for methanol synthesis from hydrogenation of either CO or CO_2. Owing to the increasing emissions by the increasing population and human activities, the concentration of CO_2 in the atmosphere is rising year by year which causes significant climate change. The attempts to reduce the CO_2 emission and develop various technologies for CO_2 capture and transformation are elevated. It has been recently reported that by utilizing solar energy, hydropower, wind power, and biomass, renewable hydrogen can be produced at large scale[1,2]. Therefore, the recycling of CO_2 through its hydrogenation to high-energy-content fuels such as alcohols or hydrocarbons appears to be very attractive[3]. Particularly, the CO_2 hydrogenation to methanol is becoming a strategically important process due to the positions of methanol as both chemical platform and clean fuel, as stated in the "methanol economy" by Nobel Laureate George Olah and co-workers[4].

A Cu surface is generally accepted to provide active sites for the catalytic CO_2 hydrogenation to methanol. Its catalytic activity is a function of surface area to volume ratio (inversely proportional to the particle size) due to the fact that catalysis is a surface phenomenon[5,6]. Thus, the generation of small Cu particles and their stabilization against Cu sintering under reaction conditions are the important aspects for the catalyst development. Despite the fact that many efforts have been made aiming to investigate how a solid precursor can control the formation of metal atoms, the fine control to the size of metal atoms and their subsequent aggregation in its matrix remain challenging. On the other hand, Cu/ZnO based catalysts are commonly applied for methanol synthesis from CO_2/H_2 and have been extensively investigated in the literature. However, the role(s) of Zn on the stabilization and activity of Cu nanoparticles are still in

debate[7–14]. Due to the rapid development of advanced characterization techniques, many reports have indicated that a very small quantity of Zn atoms is reduced on small Cu nanoparticles which results in a subtle change in geometric and electronic structure of Cu due to desirable bimetallic properties[15–18]. Consequently, it has been proposed that highly active Zn-Cu alloy is the key catalytic site[18]. In contrast, other people believe that the reaction happens at the atomic interface between ZnO and Cu, hence the presence of ZnO-Cu interfacial sites and the synergy of Cu and ZnO are important for methanol production[19]. Apart from ZnO, it is demonstrated that the incorporation of other additives, such as Al_2O_3, SiO_2, ZrO_2, and Ga_2O_3 can further enhance the activity, stability, and thermal resistance compared with the unmodified Cu/ZnO[20–25]. Particularly, the incorporation of Ga has attracted a considerably attention due to the exhibition of its higher catalytic performance. The mechanism of Ga promotion has been extensively studied, which includes the improvement of the Cu dispersion[25–27], the enhancement of electronic effect[28], the stabilization of the intermediate state of Cu[29] and the facilitation of the formation of active CuZn alloy[30], which make CuZnGa-containing catalyst a suitable candidate material for CO_2 hydrogenation to methanol.

It has been shown that monophasic catalyst precursor containing M^{2+} and M^{3+} could be obtained by controlled thermal treatment of a layered double hydroxide phase (LDH), which is a class of ionic lamellar solid often represented by the formula $[M^{2+}_{1-x}M^{3+}_{x}(OH)_2]\,(A^{n-})_{x/n}\cdot mH_2O$ with the positive divalent and trivalent metal cations located within the same layer where A^{n-} is the intercalated anion (or anions)[31,32]. Thus, it is believed that Cu^{2+}, Zn^{2+} and Ga^{3+} can also be incorporated into a stable solid LDH phase as a catalyst precursor for CO_2 hydrogenation reaction. In the literature, some studies have discussed the advantages of LDH phases as catalyst precursors[33–35], such as good dispersion of M^{2+} (Cu^{2+}, Zn^{2+}) and M^{3+} (Al^{3+}, Y^{3+} or Ga^{3+}) at an

atomic level, homogeneous microstructure, high thermal stability against sintering/reduction, high dispersion for small Cu clusters, and high specific surface area. Those benefits roused our interests in using this inorganic lamellar phase to generate Cu metal atoms within the Cu, Zn, Ga-containing cationic layer such that the active metal particles can be produced within the positively charged sheet during the reduction processes, which may reduce metal sintering between these sheets due to the local electrostatic repulsion and generate metal nanoparticles with small and homogeneous size. In addition, the recent synthesis of ultra-high surface area and high pore volume AMO-LDH phases with reduced number of cationic layers (approaching towards single-layer nanosheets) using aqueous miscible organic solvent treatment (AMOST) method[36] may further inhibit extensive Cu atom aggregation from an otherwise extended lattice. Thus, the controlled reduction of discrete, flexible but sterically separated inorganic ionic layers to produce metal atoms embedded/stabilized in the layered matrix is therefore envisaged.

In the present study, a series of Ga^{3+}-modified Cu/ZnO based catalysts ((Cu^{2+},Zn^{2+}): Ga^{3+} = 1 to 0.6) derived from AMO CuZnGa-CO_3 LDH precursors were synthesized by following the AMOST method[36]. The prepared catalysts were then evaluated for methanol synthesis from CO_2 hydrogenation and the results were compared with CuZnGa catalysts derived from conventional hydroxyl-carbonate phases (CZG samples) consisting of comparable metal contents[30,37]. In order to better understand and design the highly active catalysts for CO_2 hydrogenation to methanol, the precursor structures and physico-chemical properties of the catalysts were investigated in detail and correlated with corresponding catalytic activities. In addition, the surface state and compositions of the catalysts were studied by XPS after the reduction process to get the insight into active copper and zinc species.

Results and Discussion

Structural Characterization

With the introduction of Ga^{3+} into Cu/ZnO catalyst, a series of Cu, Zn, and Ga-containing hydroxyl-carbonate precursor phases, denoted by CZG, have been prepared using a simple and conventional co-precipitation method[30]. The procedure for the synthesis of CZG precursors can be found in Fig. S1 of the Supporting Information (SI). From the XRD patterns (phase symbols and powder diffraction file, PDF numbers are shown in SI Table S1), a dominant, aurichalcite phase of $(Cu,Zn)_5(CO_3)_2(OH)_{16}$ with a high dispersion of Ga species from 0, 5, 10% Ga concentration are seen in Fig. 1a for the freshly prepared samples. At the Ga concentrations of 30 or 40 mol%, zinc-containing malachite phase of $(Cu,Zn)_2(CO_3)(OH)_2$ is preferably formed. The formation of these two hydroxyl-carbonate phases has been widely reported in the literature using similar co-precipitation preparation method[7,30,37–40]. The peak broadening in the XRD patterns with the increase in Ga concentration provides evidence of the use of Ga to reduce the crystal size of aurichalcite phase. Particularly, at 30-40% Ga, the switch of the dominant aurichalcite phase to malachite phase is interesting. It was found that the type of precursor would sequentially vary as malachite to aurichalcite with increasing ZnO content[7]. Therefore, the switch of the dominant phase observed here is because of the decrease in Zn concentration when increasing Ga in the synthesis process (see SI Table S2). Upon calcination at 330 ^oC (Fig. 1b), bulk phases of CuO and ZnO are clearly identified in the sample with the absence of Ga. As long as Ga is included, a spinel phase of MGa_2O_4 (M = Zn/Cu) readily emerges together with minority phases of ZnO/CuO, which are stabilized over the whole Ga range of 5-40%.

On the other hand, as can be seen in Fig. 1c that samples prepared by AMOST method (synthesis procedure can be found in SI Fig. S2) via basic solution produced phase pure $((Cu,Zn)_{1-x}Ga_x)(OH)_2(CO_3)_{x/2}.mH_2O.n(C_3H_6O)$ {AMO CuZnGa-CO_3 LDHs} with increasing crystallinity at or above 20% Ga. The Bragg reflections at 2θ *ca*. 12°, 24°, and 35° were attributed to (0 0 3), (0 0 6), and (0 0 9) crystal planes in the layered structure with a rhombohedral symmetry (R3)[41]. The rhombohedral symmetry of LDH30Ga was further confirmed by synchrotron XRD analysis (see SI Fig. S3a) revealing the lattice parameters of *a*, *b* = 3.11 Å, *c* = 22.64 Å. In addition to intense Bragg reflections at 2θ = 12°, 24°, and 35°, the broad and asymmetric reflections were also observed at 2θ = 36°, 39°, and 47°, ascribed to (0 1 2), (0 1 5), and (0 1 8) crystal planes, respectively for the sample with the highest 40% Ga loading (SI, Fig. S3b). This indicates a homogeneous dispersion of various cations into the same hydroxide layer[42]. No other crystalline phases are observed from the AMO-LDH samples of 20, 30 and 40 mol % Ga which correspond to LDH structure of $[(Cu_{0.45}Zn_{0.41}Ga_{0.14})(OH)_2](CO_3)_{0.07}$, $[(Cu_{0.47}Zn_{0.32}Ga_{0.21})(OH)_2](CO_3)_{0.105}$ and $(Cu_{0.49}Zn_{0.22}Ga_{0.29})(OH)_2(CO_3)_{0.145}$, respectively according to the ICP analyses (SI Table S2). The discrepancy between nominal and ICP-measured Ga content in the samples is from the loss of metal ions dissolved in the solution during the filtration process of the co-precipitation method. It is noted that using 30 mol% Ga in the synthesis recipe is appropriate to form ultra-thin AMO-LDH sheets (by the AMOST method) than the other two AMO-LDH samples (20% and 40% Ga) as the stability of LDH structure depends critically on the overall charge of the cationic layer with specific M^{3+}:M^{2+} ratio balanced with intercalated anions[43]. For example, the cationic charge for the layer holding the higher ratio of M^{2+}/M^{3+} = 4 (20 mol% Ga^{3+}) is anticipated to be at the lower end of the stability range; hence, it may be relatively unstable and form amorphous precipitates such as hydroxides and hydroxyl-carbonates in the presence of AMO solvent[41].

Below the critical 20% Ga concentration, amorphous phase is clearly recorded. Similarly, adding 40 mol% Ga in the synthesis ($M^{3+}/M^{2+} > 0.5$) leads to stronger electrostatic interaction between the layers due to the presence of higher amount of stoichiometric intercalated carbonate anions. This creates thicker LDH layers (see SI Fig. S3b and Fig. S4a), which is difficult to disrupt (exfoliate) by the AMO solvent treatment. Notably, calcination of the AMO-LDHs at 330 ^{o}C did not reveal any formation of spinel structures or metal oxides from XRD investigation (Fig. 1d). This clearly indicates that LDHs have a kinetically more stable phase than the conventional hydroxyl-carbonate phases (CZG samples). LDHs normally have two typical distinct thermal events at around <200 ^{o}C (noted as T1) and 500-600 ^{o}C (noted as T2) evaluated by thermogravimetric analysis (see SI, Fig. S4b). The weight loss below T1 is due to the desorption of physisorbed and intercalated solvents and water. After T1, the hydroxyl groups start to decompose and gradually transform the LDH structure to a reversible amorphous phase. This reaches a maximum at 550 ^{o}C (T2), and is ascribed to the partial decomposition of carbonate anions and complete dehydroxylation of the metal hydroxide layers[36]. Thus, the applied calcination temperature of 330 ^{o}C gives mainly the amorphous phase with probably a trace amount of layered double oxides (LDO, although not detected in this work) without reaching the second stage of the layer structure collapse.

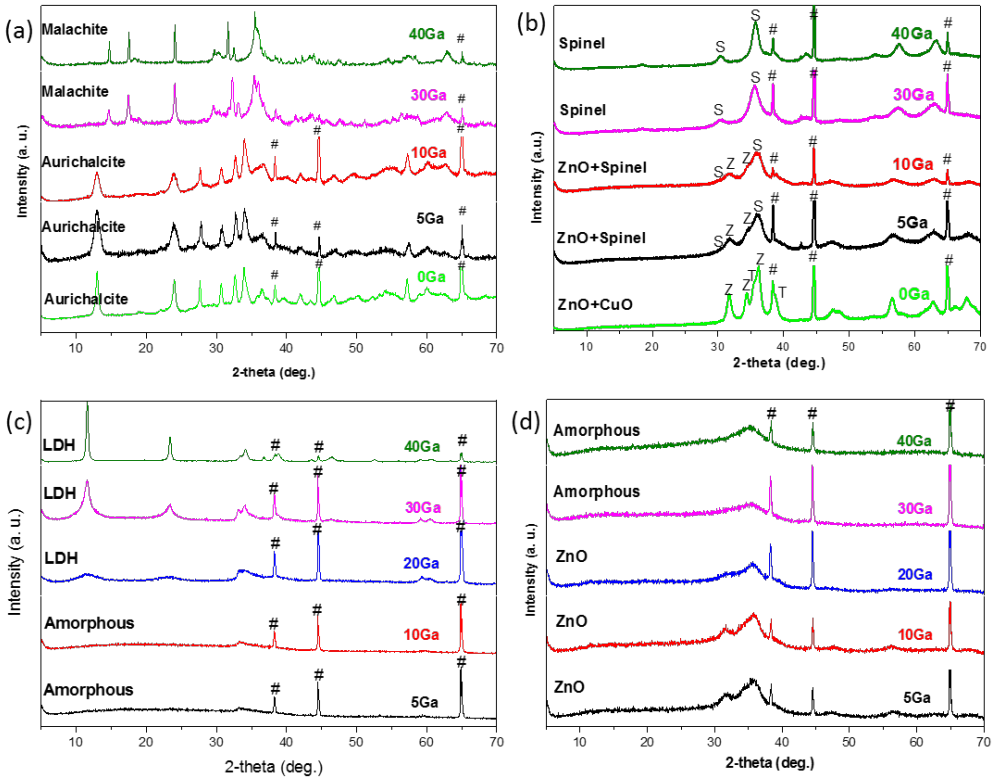

Figure 1. XRD profiles of (a) freshly prepared CZG catalysts; (b) calcined CZG catalysts at 330 ^{o}C; (c) freshly prepared AMO-LDH samples; (d) calcined AMO-LDH samples at 330 ^{o}C (# peaks from Al holder; S: spinel phase; T: tenorite phase; Z: zincite phase).

Morphology Analysis of the Precursors

In order to determine the textural properties of these samples, TEM and AFM were employed. Fig. 2a and 2b show the typical images of the hydroxyl-carbonate phase of CZG5Ga and CZG40Ga prepared by co-precipitation method. It appears that the extended fibrous/sheet-like structure in the lower Ga content is fragmented in the presence of a high Ga concentration, giving many smaller particles. On the other hand, the LDH5Ga is similar in textual appearance

as CZG5Ga although small sheet-like features are occasionally observed (Fig. 2c). It is noted that the XRD patterns of the AMO-LDH samples with low Ga concentration (LDH5Ga and LDH10Ga) in Fig. 1c show no indication of LDH phase formation, which is not surprising. Their M^{2+}:M^{3+} is outside the stability range for LDHs, but probably some mixed phases of hydroxyl-carbonate structures of below the detection limit by the XRD are made, hence giving mixed shapes (particles/fibrous/sheets) in appearance. At 20% Ga (M^{2+}/M^{3+} = 4) or above, sheet-like structures are observed (see typical Fig. 2d), which agrees with the expected layered LDH structure identified by the XRD (Fig. 1c). More TEM images of freshly prepared CZG samples and AMO-LDH samples can be found in SI Fig. S4a.

The striking reduction in the number of cationic layers via acetone (AMO-solvent) inter-layer disruption produced by the AMOST method (fine particle portion) can be identified by AFM on the 30% Ga (M^{2+}/M^{3+} = 2.33) sample (Fig. 2e). As can be seen from Fig. 2f that the typical height profile of LDH30Ga sample clearly shows a thickness between 0.8–2.3 nm for selected regions, which corresponds to 1–3 layer LDH platelet according to our 3-layer LDH30Ga structural model intercalated with carbonate anions as depicted in Fig. 3 (for the single cationic layer, the structure stabilized by adsorbed carbonate anions is anticipated). The formation of such ultra-thin CuZnGa nanosheets which are separated by discrete cationic layers and balanced by intercalated carbonate anions suggests that acetone dispersion can override the weaker interlayer electrostatic interaction, thus accounting for the dramatic increase in surface area of this sample.

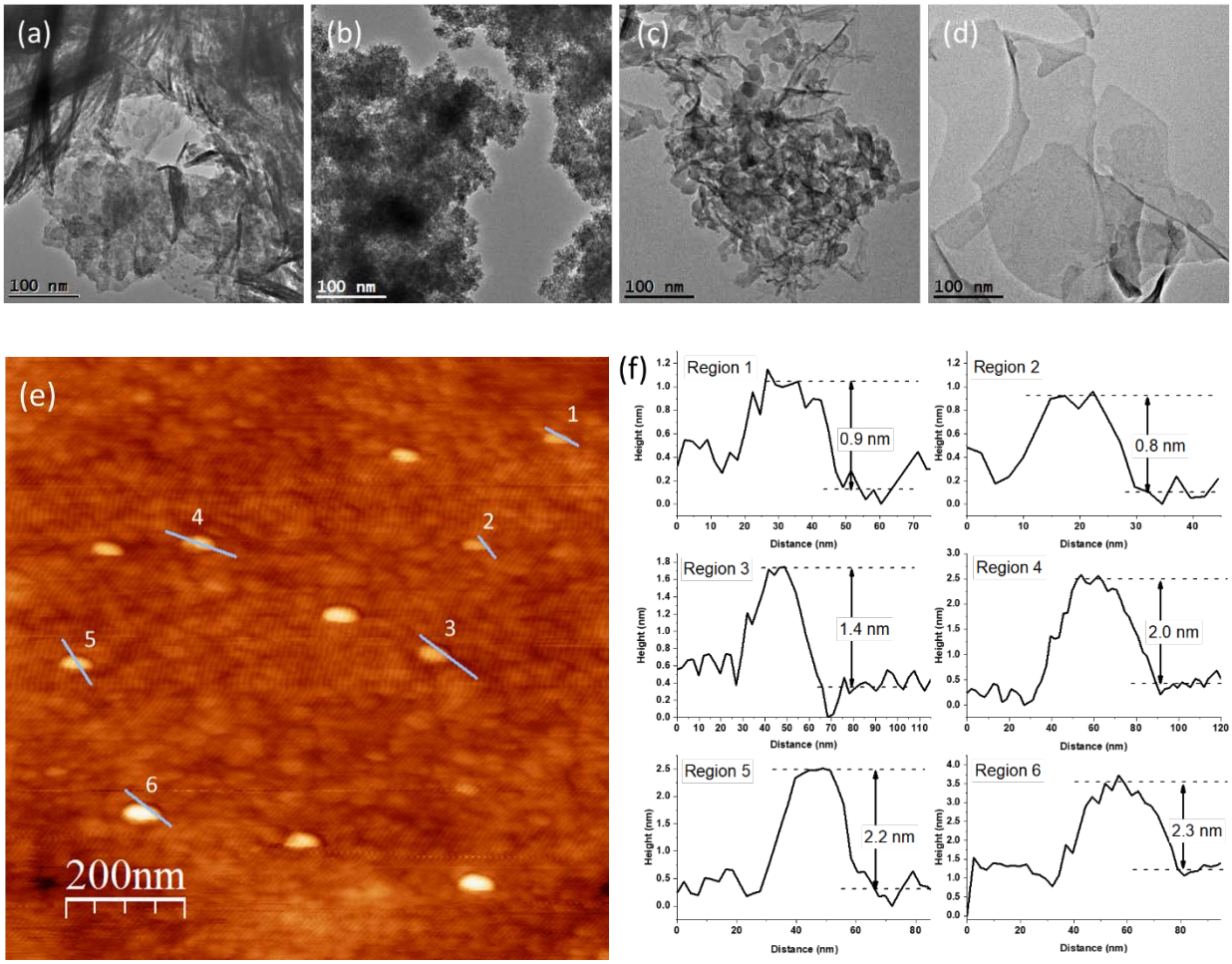

Figure 2. TEM (a-d) images of freshly prepared CZG and AMO-LDH samples: (a) CZG5Ga; (b) CZG40Ga; (c) LDH5Ga; (d) LDH30Ga**;** (e) AFM image of single layer and few layers freshly prepared LDH30Ga sample on Si substrate and (f) the height profile of (e).

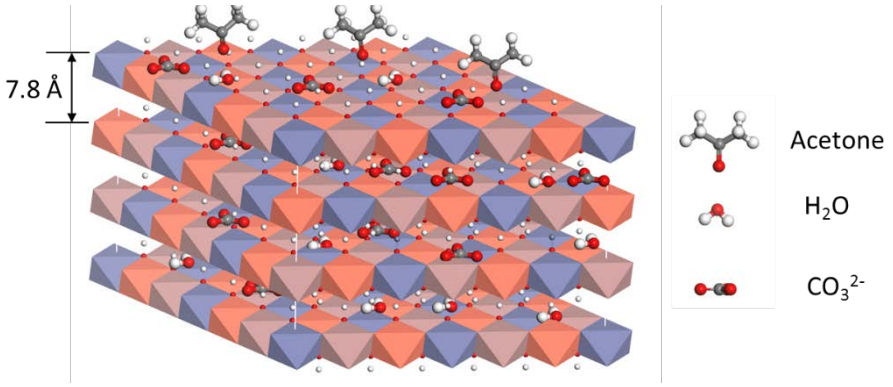

Figure 3. The LDH30Ga structural model showing 3 cationic layers with intercalated carbonate anions and water molecules in between. Each cationic layer contains Cu^{2+} (blue), Zn^{2+} (grey) and Ga^{3+} (orange) with OH^{-} vertexes in face-sharing octahedra with an inter-layer separation of 7.8 Å in a rhombohedral (3R symmetry) $[(CuZn)_{1-x}Ga_x(OH)_2](CO_3)_{x/2}$ LDH structure derived from synchrotron XRD data (SI Fig. S3). For simplicity, equal population of Cu, Zn and Ga ions are presented in this model and Jahn-Teller distortion of Cu^{2+} in octahedral sites is also not shown.

Investigation of Reduction Behavior and Active Cu Surface Area

The reduction behaviour of calcined CZG and AMO-LDH samples was investigated by H_2-TPR, and the corresponding reduction profiles are given in Fig. 4. It is known that Cu^{2+} has the more favorable reduction potential than the other two metal cations, i.e., Zn^{2+} and Ga^{3+}. The TPR analysis show that all samples give virtually the same integral reduction peak area of 5.0 ± 0.5 mmol $H_2 \cdot g_{cat}^{-1}$ corresponding to the complete reduction of Cu^{2+} to Cu^0. It is, however, interesting to note from Fig. 4a that CZG samples display a complex and broadened reduction peak accompanied by shoulders in the temperature range of 150–270 ^{o}C. This indicates that some reduced Cu species exist in heterogeneous chemical environments (variation in size and structure), thus leading to different peak maxima at different reduction temperatures. The

reduction range of 150–200 ^{o}C (low temperature shoulder) matches with that of Cu_2O but its content in CZG samples diminishes at higher Ga loading[25,37]. The higher temperature main peak is attributed to the broad reduction of $CuGa_2O_4$ and CuO phases of different sizes. Such a large variation in reduction behaviour of Cu^+ and Cu^{2+} in heterogeneous mixture of extended lattices would expect to induce large Cu particle size variation in the CZG precursor-derived catalysts. Without Ga, even higher temperature is required for the complete Cu^{2+} reduction, which gives inefficient utilization of Cu active sites from the CZG precursor samples under dynamic reaction conditions. On the other hand, the reduction profile of LDH samples shown in Fig. 4b displays more uniform and sharper peak profiles but at a higher temperature range of 200–290 ^{o}C. Comparing to the CZG samples, the LDH samples do not show low temperature shoulder peak (absence of Cu_2O), therefore, more homogeneous Cu particles are expected to generate from the reduction of ultra-thin LDH phase prepared by the AMOST method. On the other hand, the thick LDH40Ga sample (see TEM image in SI Fig. S4a) with stronger interlayer charge density requires much higher reduction temperature to reduce the Cu atoms.

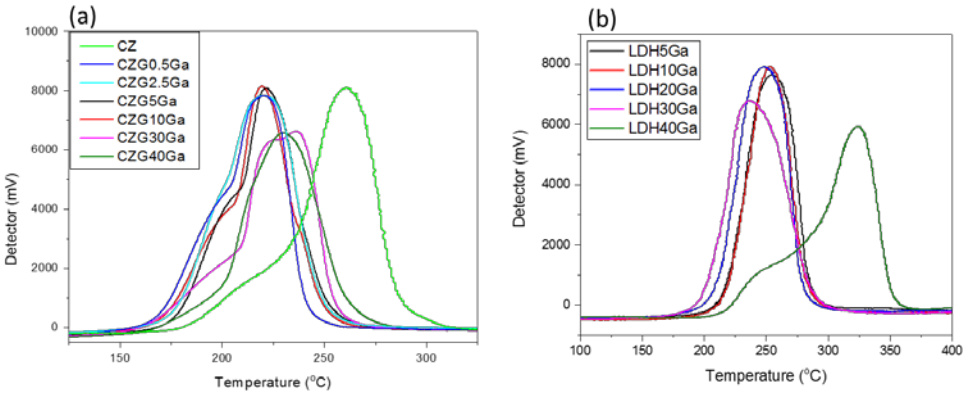

Figure 4. Temperature Programmed Reduction (TPR) profile of calcined (a) CZG samples (b) LDH samples.

The Cu loading (determined by ICP), Cu dispersion and Cu surface area (determined by N_2O chemisorption) for the Cu-containing CZG and LDH catalysts were determined accordingly and are shown in Table 1. It is noted that the absolute values for Cu dispersion and Cu surface area determined by N_2O should not be taken too literally. This is because recent studies have clearly shown that N_2O is not just oxidizing the copper surface but also oxidizing other reduced species, i.e., Zn or oxygen vacancies on support[44–46]. However, it is clear from the compiled Cu surface areas and Cu dispersions that CZG samples give consistently lower values than LDH samples, which agree with a similar behaviour as observed from the BET surface area analysis that CZG precursors have much lower specific surface areas than the AMO-LDH precursors (see SI Fig. S1 and S2). In addition, it is noted that the LDH precursor without AMO solvent treatment, LDH30Ga-ww, shows much lower BET surface area compared to LDH30Ga prepared via AMOST method, indicating the solvent exfoliation process is very crucial for producing high surface area ultra-thin LDH structures. Further information can be found in SI Fig. S5 where the nitrogen adsorption-desorption isotherms and a discussion on the porosity of the selected CZG and LDH samples are presented.

Table 1. Comparison of Cu loading, Cu dispersion, Cu surface area for the Cu containing CZG and LDH derived catalysts.

Catalysts	Cu loading[a] (wt%)	Cu dispersion[b]	S_{Cu}[b] (m^2/g_{cat})
CZ	33.4	21.8	43.0
CZG5Ga	31.9	22.0	45.2
CZG10Ga	33.9	19.5	42.7
CZG30Ga	32.7	19.6	41.3
CZG40Ga	33.5	21.1	45.5
LDH10Ga	34.3	24.4	53.8
LDH20Ga	33.4	33.8	72.8
LDH30Ga	33.5	46.0	99.2
LDH40Ga	37.9	22.6	55.3

[a] Determined by ICP; [b] Dispersion and specific surface area of metallic Cu determined by N_2O chemisorption.

Catalyst Screening and Correlation Between Activity and Structural Parameters

The catalytic performances of Cu-containing CZG and AMO-LDH precursor samples for methanol production via CO_2 hydrogenation were evaluated and are presented in Fig. 5, SI Fig. S6 and S7. The main product for all catalysts demonstrated here is methanol with CO as the only by-product under the reaction conditions of H_2 : CO_2 (molar) = 3 : 1, T = 190–310 ^oC, P = 4.5 MPa and WHSV = 18,000 $mL \cdot g_{cat} \cdot h^{-1}$. The activity measurements were taken after at least 2 h on stream at each selected temperature. Similar catalytic performances of CZ and CZG samples were observed in terms of CO_2 conversion, probably, due to their similar Cu content, Cu surface areas and dispersions, see Table 1. However, differences were identified in their selectivities toward methanol. In general, the methanol yields of CZ and CZG catalysts (SI Fig. S6) increase with the increase in temperature and reach the optimal value of about 290 ^oC before they are

rapidly attenuated due to the thermodynamic constraints. It can be seen in Fig. 5a that among all CZG samples, CZG5Ga reveals the best performance. The addition of 5 mol% Ga into CZ leads to an increase in CH_3OH selectivity and yield, but further increase of Ga content starts to decrease the activity where the performance of CZG40Ga is even lower than the CZ catalyst. The interpretation of these data is not straightforward because there is no general trend for CZG samples that correlates to the small variations in Cu dispersion and S_{Cu} (SI Fig. S8a). This observation suggests that the catalytic conversion of CO_2 to methanol of the CZG sample may not only be dependent on copper surface area but also on other factors, presumably on structural and compositional differences of nanoparticles (structural sensitive). Indeed, our previous study[47] revealed that adding Ga into Cu/ZnO system could change the surface Zn^0 concentration, which was proven to have a strong correlation to the catalytic performance of methanol production from CO_2 hydrogenation. In addition, TEM (Fig.2 and SI Fig. 4a) and XRD (Fig.1) results show that there is a large morphological and structural variation in the CZG precursors with different Ga addition, which might also have influences on the catalytic properties of the CZG catalysts.

Similar to CZG samples, CO_2 conversion of AMO-LDH precursor catalysts increases with the increase in temperature while selectivity of methanol declines (SI Fig. S7). In addition, methanol yield of the homogeneous LDH-based catalysts also presents a volcano trend with increasing temperature: Most of the LDH catalysts reach the optimal methanol yield at 290 ^oC, which is the same optimal reaction temperature as in the CZG samples, but LDH30Ga and LDH20Ga catalysts exhibit methanol yield maxima at a lower temperature (270 ^oC). With the increase of Ga content, the catalytic activity increases and reaches the maxima at LDH30Ga sample. It can be seen from Fig. 5b and Fig. 1c that the catalytic activity for the catalysts via ultra-thin LDH precursors was better than that for the catalysts derived from amorphous precursors (below 20%

Ga addition). According to Fig. 5b and SI Fig. S8a, the LDH samples which show higher Cu surface areas and Cu dispersions, particularly the LDH20Ga and LDH30Ga, also give higher methanol selectivities and yields. However, further increase of the Ga^{3+} to 40% results in a significant drop on the CO_2 conversion, presumably due to the formation of well-crystallized LDH phase with the compaction of platelets that can be observed by TEM (thick LDH layers, see SI Fig. 4a), leading to a decreased amount of exposed Cu on the surface of the reduced catalyst. In addition, from the H_2-TPR result (Fig. 4b), LDH40Ga sample requires much higher reduction temperature to reduce the Cu atoms, which gives inefficient utilization of Cu active sites from the precursor when employing the same reduction temperature (290 ^oC) as other samples. Among all the catalysts, the best performance is obtained by LDH30Ga which gives nearly 9% methanol yield. This matches with the general consent from the literature that Cu surface primarily provides active sites for this hydrogenation reaction[5–8]. Therefore, with an appropriate incorporation of Ga^{3+}, the formation of ultra-thin LDH phases could improve the dispersion and the surface exposure of active Cu, giving rise to a better catalytic performance for CO_2 hydrogenation to methanol. After 25 hours on stream at 290 ^oC and 4.5 MPa, see SI Fig S9, LDH30Ga shows no obvious deactivation (only a slight decrease of methanol yield by 0.2% from 6h to 25h on stream), indicating the catalysts derived from the ultra-thin LDH structures produced via AMOST method are fairly stable.

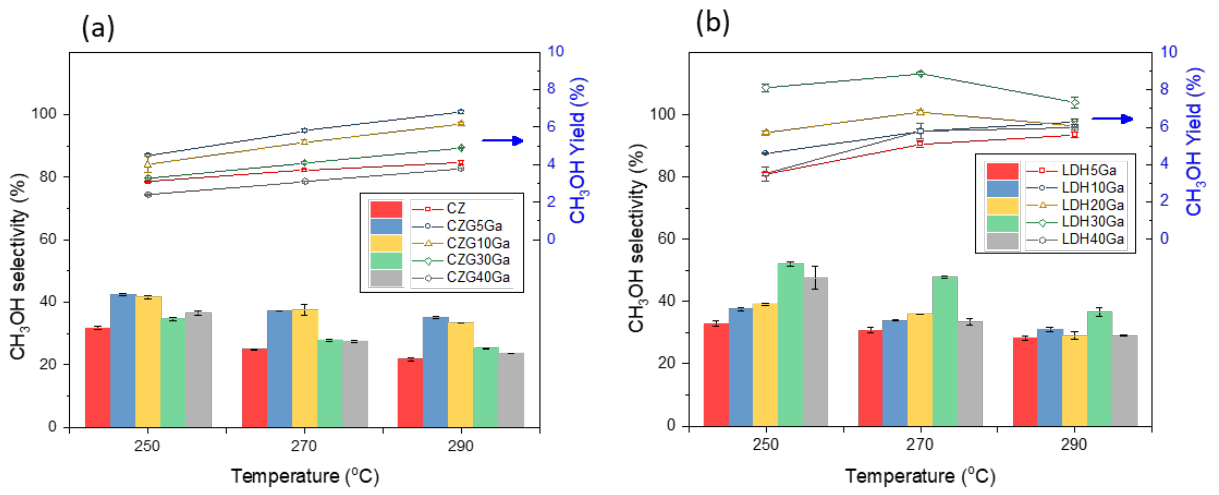

Figure 5. Catalytic performance of CZG (a) and AMO-LDH (b) precursor catalysts for CO_2 hydrogenation to methanol. Reaction conditions: T = 190–310 °C, P = 4.5 MPa, WHSV = 18,000 $mL \cdot g_{cat}^{-1} \cdot h^{-1}$, and H_2:CO_2 (molar) = 3:1. For simplicity and clarity, only 250–290 °C temperature range, at which the catalysts exhibited higher activity, is presented. Error bars indicate the standard deviation of the raw data.

To find out the correlation of the intrinsic activity of the CO_2 hydrogenation to methanol to the amount of the exposed Cu on the catalyst surface, the turnover frequency (TOF, s^{-1}), which represents the number of methanol formation per exposed copper atom per second, was calculated using the number of the surface Cu sites evaluated by N_2O chemisorption. TOF as the function of Cu surface area (S_{Cu}^0, m^2/g_{cat}) is shown in SI Fig. 8b. Comparing the results to the literature, the TOF values of the CZG and AMO-LDH samples are at the medium of those in the Cu-based catalysts[18,48–50]. It can be seen from Fig. 8b that CZG samples present TOF values in the order of CZG5G > CZG10Ga > CZG30Ga > CZ > CZG40Ga within a narrow S_{Cu} range of 40-50 m^2/g_{cat}. As mentioned previously[30], the activity of CZG mainly depends on the surface

concentration of Zn^0, hence no obvious relationship can be found between TOF and Cu surface area. On the contrary, AMO-LDH samples show that the TOF decreases slightly with increasing S_{Cu}, and similar trend has been reported by other researchers[20,49,50]. Many researchers proposed that the synergy between Cu–Zn (or ZnO) and the Cu/oxide support interaction are essential to ensure high TOF in methanol synthesis from CO_2/H_2[18,19]. Recent work further indicates that the increase in TOF for Cu/ZnO based catalysts is mainly due to the formation of partially reduced zinc species on the copper surface[18]. In addition, it was suggested that the defective step edges on Cu surface are the active sites, but such unique configuration of Cu step sites were found to be unstable in too small particles (high Cu dispersion/surface area, as the surface areas and dispersions are inversely proportional to the particle size), thus lower TOF values were observed when the particle size decreased[18,51]. Therefore, the slightly lower TOF value of the LDH30Ga could be the result of its extremely high dispersions and surface areas of Cu. However, a high Cu dispersion/surface area is generally accepted as a prerequisite for good activity, and enhancing Cu dispersion/surface area is one of the major goals for Cu-based catalyst preparation[40,52]. With such high population of active Cu working altogether on the surface, the LDH30Ga sample can perform superiorly compared to other catalysts.

Recently, the effect of the Cu particle size has been found to be strong to the catalytic CO_2 hydrogenation reaction[51]. Therefore, the particle size of the active species in both CZG and AMO-LDH systems were further investigated. Fig. 6a shows that after calcination in air atmosphere, the formation of mixed metal oxides (appeared as sphere-like particles) in the calcined CZG5Ga sample can be observed. Fig. 6b–6d show the images of the reduced CZG5Ga sample prepared with H_2 treatment at 290 ^oC (2 h), which give 5–10 nm Cu-rich particles with occasionally much larger particles (> 10nm) observed. In contrast, the image of calcined

LDH30Ga (Fig. 6e) reveals multiple curved sheets assembled mostly of single discrete layers with some edge regions of 2–3 staggered layers. This indicates the AMO-LDH precursor is very stable, which can maintain its ultra-thin layered morphology in spite of exhibiting an amorphous phase (Fig. 1d) after calcination. Under identical hydrogen treatment shown in Fig. 6f–6h, many small and rather homogeneous size Cu-rich particles of less than 5 nm (mean size = 4.0 ± 0.1 nm) are formed on this positive charged sheet-like structure. More TEM images of reduced CZG5Ga and LDH30Ga can be found in SI Fig. S10. In line with the morphology observation of the reduced catalysts, the reduction behaviour of the AMO-LDH samples, see Fig. 4, displays more uniform peak profiles compared to the CZG samples, implying a more homogeneous reduction environment in the AMO-LDH matrix. The controlled reduction with the formation of smaller Cu seeds in the AMO-LDH sample clearly reflects that Cu species must be engaged in a stable LDH structure, which offers the fine controlled nucleation and restricted mobility of metal atoms by the high surface and discrete inorganic nanosheets, thus can lead to small and homogeneous Cu particles upon H_2 reduction process. Recently, Van Den Berg *et al.*[51] have extensively tested a range of supported Cu particles from 2–15 nm and found that smaller Cu particles are more active for CO/CO_2 hydrogenation to methanol but too small Cu particles such as 2 nm show poorer activity, which is attributed to the lack of active step-edge sites and the subtle change in local electronic structure for such small metal particles. On the other hand, Van Helden *et al.*[53] have computed for cobalt face-centred cubic particles that similar to Cu, the active site fraction of step sites (so-called B5) increases with increasing particle size until 4 nm. We believe the formation of Cu nanoparticles in the catalytically active size domain with narrow size distribution is related to a delicate control of nucleation and growth. For the AMO-LDH derived catalysts, the discrete cationic layer with high charge density appears to offer the

required steric and electrostatic stabilization, which is advantageous to make larger Cu surface area with higher metal dispersion (4 nm particle size) upon reduction. In this respect, Cu containing AMO-LDH samples are superior to those prepared by the conventional co-precipitation method.

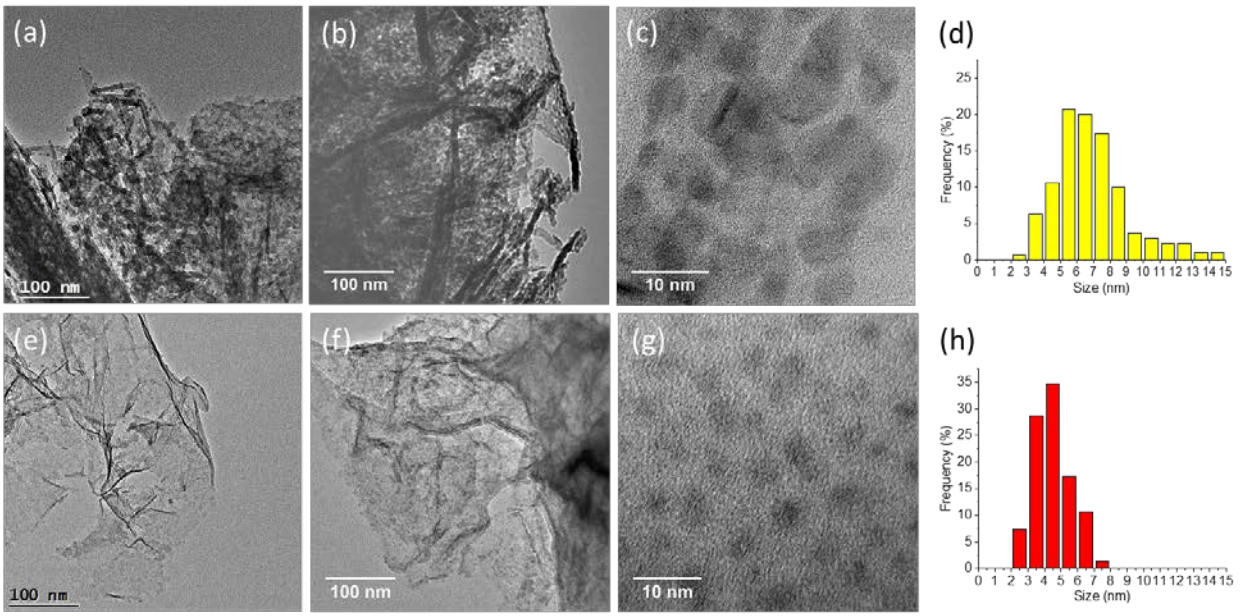

Figure 6. TEM images of the calcined (a, e) and reduced (b, c, f, g) samples, and size distribution diagrams (d, h) of the nanoparticles in the reduced samples. Upper rows: (a) calcined CZG5Ga; (b-d) reduced CZG5Ga containing 5–10 nm Cu-rich particles (mean size = 6.3 ± 0.2 nm) with some of much larger sizes. Lower rows: (e) calcined sheet-like LDH30Ga sample; (f-h) reduced LDH30Ga containing many homogeneous small Cu-rich particles of < 5nm (mean size = 4.0 ± 0.1 nm).

The XPS results of the reduced AMO-LDH samples with various Ga contents are revealed in Fig. 7. Fig. 7a clearly shows the progressive increase in Ga peak area at increasing Ga content. In comparison with the peak position with reference to the C 1s transition at 285 eV, Ga is still maintained as Ga^{3+} with no sign of reduction[54]. However, the positions of $2p_{1/2}$ and $2p_{3/2}$ signals of Cu (Fig. 7b) match well with those of Cu^0 and their peak sizes remain the same at increasing Ga concentrations. This again suggests that Cu^{2+} is totally reduced from the AMO-LDH samples upon the pre-reduction treatment under H_2 at 290 ^oC. Although there is no systematic trend observed from the XPS peak positions of Ga 2p and Cu 2p, a slight peak shift, especially the LDH30Ga, can be observed. It is known that the exact binding energy of an electron depends on several factors including the oxidation state of the atom, the local chemical and physical environment, particle size, and charge transfer within two elements in the contact region. Therefore, the peak shifts observed in the AMO-LDH samples from both Ga 2p and Cu 2p could be attributed to the morphological changes as the formation of pure-LDH phases from amorphous (when Ga > 20%), and the following changes in platelet thickness/size when further increasing the Ga content. Moreover, the charge transfer between Zn and Cu upon the reduction of Zn species (will be discussed later) may also be one of the parameters that contribute to the Cu 2p peak shift. The peak position of Zn $2p_{3/2}$ shown in Fig. 7c of AMO-LDH samples matches with Zn^{2+} indicating that most of these cations remain unreduced in the solid structure. However, there is a small degree of Zn^{2+} reduction to Zn^0 at Ga concentrations of 20 and 30 mol% which correspond to the precursors with pure-LDH phases as well as high surface areas. Through careful deconvolution, the broader peak can be separated into two sub-peaks of Zn^{2+} (1023 eV) and Zn^0 (1021 eV). The differentiation between Zn^{2+} and Zn^0 in XPS spectra is regarded as a challenging task because the difference of peak positions between Zn^{2+} and Zn^0 is not very

evident. However, it is clear that the AMO-LDH samples with a trace amount of Zn^0 from ZnO (LDH20Ga and LDH30Ga) show better methanol production rate, indicating that the active CuZn sites can be formed in the AMO-LDH samples, which exerts the enhancement to the catalytic reaction. In the literature, it has been suggested that Cu/Zn interface plays a significant role in CO_2 hydrogenation to methanol as these two species (Cu and Zn) work synergistically. Thus, placing Zn in a proximity to Cu can enhance methanol synthesis[18,30,46]. Catalysts containing Cu/ZnO were recently found to show 10 times higher activity than Cu catalysts of the same sizes but without in contact with ZnO[51]. This agrees with our observations that this composition modification is a very important one. However, many models have been put forward in the literature to explain the role of zinc, including zinc-induced defects in the copper structure[55], hydrogen spillover from zinc oxide to copper[56], the electronic stabilization[57,58], and the morphological control on Cu nanoparticle[59]. Behrens *et al.*[18] reported that the increase in activity for zinc-containing catalysts is mainly due to the formation of reduced zinc species from zinc oxide and subsequent migration to copper surface. By using density functional theory (DFT) calculations, their work has indicated that a higher Miller-index copper surface, Cu(211) contains active step sites, can be favorable decorated with Zn metallic atoms rather than on the Cu(111) terrace surface. This exerts a strong electronic effect on Cu phase in this reaction. In the present study, the formation of a trace amount of Zn^0 atoms (shown in XPS result) upon co-reduction for the decoration on small and homogeneous Cu nanoparticles made by LDH30Ga sample seems to support their conclusion.

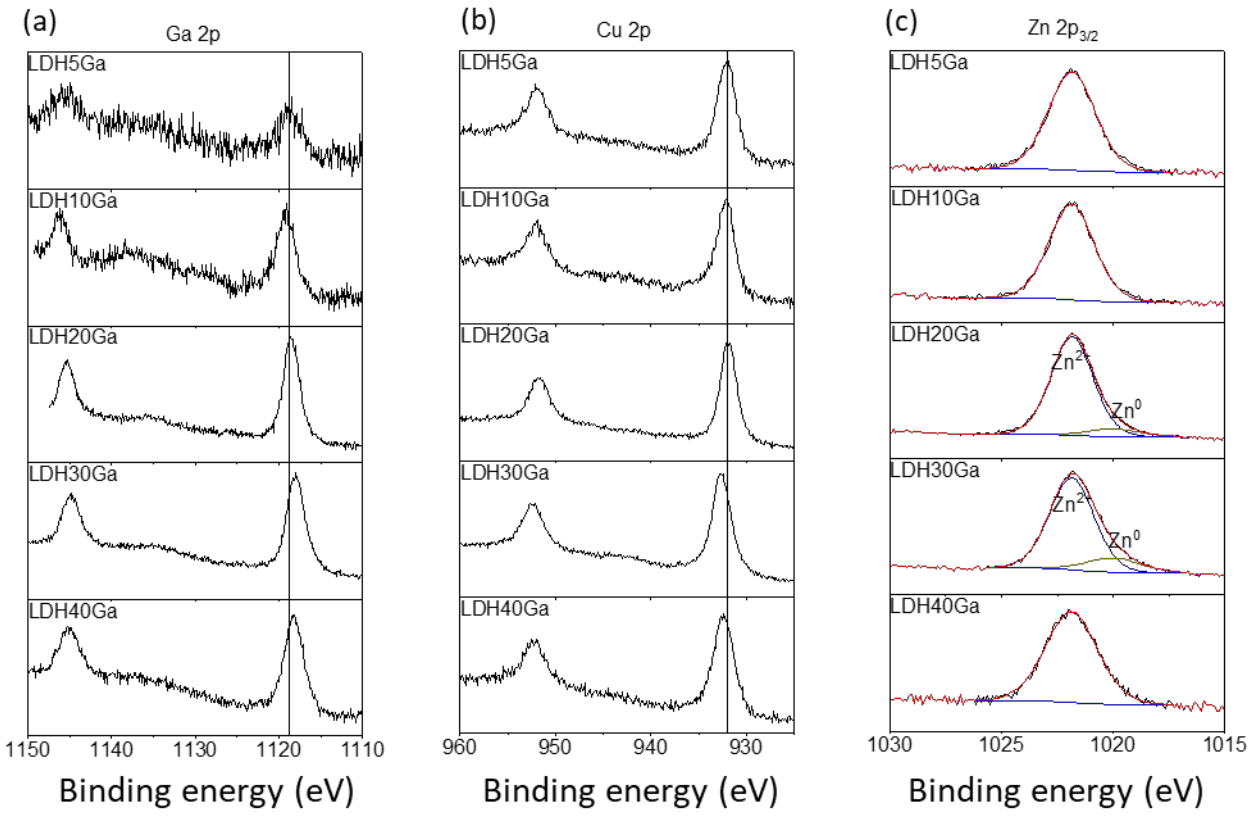

Figure 7. XPS spectra of the reduced AMO-LDH derived samples of (a) Ga 2p peaks; (b) Cu 2p peaks; (c) Zn 2 $p_{3/2}$ peaks at various Ga concentrations.

Comparison of Catalytic Activity

The catalytic performances of CZG5Ga, commercial HiFUEL^{TM} catalyst (Johnson Matthey, plc), and LDH30Ga with and without acetone treatment which contain comparable Cu loadings have been compared in Fig. 8. It is apparent that the LDH30Ga sample (dispersed with acetone) reveals the best performance among the four samples. As stated[36], when the final wet slurry of LDH was dispersed with an AMO solvent (acetone), it dramatically enhances the surface area of the final material ($S_{LDH30Ga}$ =158.71±0.17 m^2g^{-1} vs $S_{LDH30Ga\text{-}Ww}$ = 36.51±0.10 m^2g^{-1}, see SI Fig.

S2) by exfoliating the cationic multilayers (intercalated with carbonate anions) approaching to 1–3 layers. This discrete cationic layer can facilitate the formation of small (~4 nm) and homogeneous Cu particles decorated with trace Zn atoms with narrow size distribution, which lead to higher CO_2 conversion and methanol production. In comparison with other reported catalysts using ternary or quaternary Cu-containing LDH as the precursors without AMO solvent exfoliation[41,60–62], our simple AMO-LDH (LDH30Ga) precursor catalyst shows greater methanol production rate (see Table 2). Moreover, the AMO-LDH catalyst is also superior to those reported Cu-Zn-Ga catalysts prepared via different methods including impregnation methods ($Cu\text{-}ZnO\text{-}Ga_2O_3/SiO_2$)[29] and microwave-assisted method ($(CuZnGa)_{MW}$)[63]. The changes of the reaction conditions are known to have a strong influence on the catalytic properties. In general, an increase of reaction pressure, H_2/CO_2 ratio, or the space velocity would favor the production of methanol in CO_2 hydrogenation reaction. Therefore, we could not provide a fair comparison of the catalytic performance of our catalysts to the catalysts reported in the literature owing to the various reaction conditions employed in different researches. However, as far as we are aware, the impressive methanol space-time yield of 0.6 $g_{MeOH}\cdot g_{cat}^{-1}\cdot h^{-1}$ of our LDH30Ga AMO-LDH catalyst at typical reaction conditions represents one of the best reported catalytic activities for methanol synthesis using Cu-based catalysts[64]. Apart from the Cu-containing catalysts, other catalyst systems with promising catalytic performance have also been extensively studied and reported in recent years. It was demonstrated that In_2O_3/ZrO_2 catalyst exhibits a very high selectivity for the conversion of CO_2 to methanol[65]. However, under the reaction conditions (pressure at 5 MPa, high H_2 : CO_2 ratios of 4–8, and high space velocity of 20,000 $mL\cdot g^{-1}\cdot h^{-1}$) that were deliberately controlled to achieve ~100% methanol selectivity, the methanol space-time yield of the In_2O_3/ZrO_2 catalyst was only ~0.3 $g_{MeOH}\cdot g_{cat}^{-1}\cdot h^{-1}$. On the other hand, it was

recently reported that ZnO-ZrO_2 solid solution catalyst is an active catalyst for converting CO_2 with high selectivity and yield toward methanol formation. ZnO-ZrO_2 solid solution catalyst was reported to show methanol selectivity of up to 86 to 91% with methanol space-time yield of 0.7 $g_{MeOH} \cdot g_{cat}^{-1} \cdot h^{-1}$ under the reaction conditions of 5.0 MPa, H_2/CO_2 = 3 to 4, temperature of 320° to 315°C, and a much higher space velocity of 24,000 $mL \cdot g^{-1} \cdot h^{-1}$ compared to that of in the present study. Additionally, when comparing our catalysts to the recently reported Pd@Zn core-shell system[66], it is surprising to see that our best AMO-LDH (LDH30Ga) catalyst gives a comparable methanol space-time yield to the highly active Pd@Zn catalysts[47] under the same reaction conditions, though Pd is commonly regarded to be more active than Cu upon modification. The methanol space-time yields of selected materials described above are compared in Table 2.

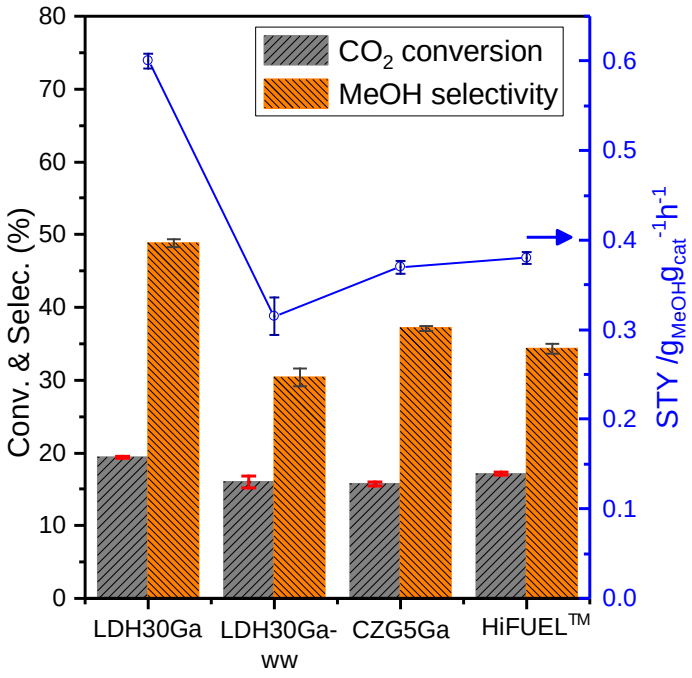

Figure 8. Comparison of conversion, selectivity and yield of CZG5Ga, LDH30Ga, LDH30Ga-ww, and an industrial sample, HiFUEL™ with comparable Cu loadings for the CO_2 hydrogenation to methanol at 270 ^{o}C. Data reported are the mean values from two replicated experiments (each has at least six data points recorded). Error bars are calculated based on the standard deviation from the mean values.

Table 2 Comparison of methanol space-time yields of selected catalysts with this work.

Catalyst	Reaction conditions			Catalytic performance	Ref.
	P (bar), T (°C)	Space velocity [a]	H_2/CO_2	STY[b]	
LDH30Ga (Cu: 33.5 wt%)	45, 270	(W) 18000 mL g^{-1} h^{-1}	3	0.59	This work
LDH30Ga-ww (Cu: 34.3 wt%)	45, 270	(W) 18000 mL g^{-1} h^{-1}	3	0.32	
CZG5Ga (Cu: 31.9 wt%)	45, 270	(W) 18000 mL g^{-1} h^{-1}	3	0.37	
JM-HiFUEL™ (50 wt% $Cu/ZnO/Al_2O_3$)	45, 270	(W) 18000 mL g^{-1} h^{-1}	3	0.38	
LDH (Cu, Zn, Al, Y) (mol % of Cu:Zn:Al:Y = 51.1:23.5:22.4:3.0)	50, 250	(W) 10000 mL g^{-1} h^{-1}	3	0.39	41
Cu on LDH (Zn, Al, Zr) supports (Nominal mol % of Cu:Zn:Al:Zr = 60:30:7:3)	50, 250	(W) 7500 mL g^{-1} h^{-1}	3	0.30	60
LDH (Cu, Zn, Al, Y) (mol % of Cu:Zn:Al:Y = 51.3:23.6:22.5:2.6)	50, 250	(W) 12000 mL g^{-1} h^{-1}	3	0.52	61
LDH (Cu–Zn–Al–Zr) (mol % of Cu:Zn:Al:Zr = 50:22:26:2)	50, 190	(G) 4000h^{-1}	3	0.087	50
LDH (Cu, Zn, Al, Ga) (Nominal mol % of Cu:Zn:Al:Ga = 50:17:18:15)	60, 250	(W) 20000 mL g^{-1} h^{-1}	H_2:CO:CO_2:He =72:10:4:14	Lower than the conventional $Cu/ZnO/Al_2O_3$	62
LDH (Cu, Zn, Al) (Nominal mol % of Cu:Zn:Al=50:17:33)	60, 250	(W) 20000 mL g^{-1} h^{-1}	H_2:CO:CO_2:He =72:10:4:14		67
$(CuZnGa)_{MW}$[c] (Cu: 16.6 wt%)	45, 270	(G) 3000 h^{-1}	3	~0.19	63
$Cu\text{-}ZnO\text{-}Ga_2O_3/SiO_2$ (Cu: 5 wt%)	20, 270	(W) 18000 mL g^{-1} h^{-1}	3	0.349	29
$ZnO\text{-}ZrO_2$	50, 320	(W) 24000 mL g^{-1} h^{-1}	3	0.73	68
In_2O_3/ZrO_2	50, 300	(W) 20000 mL g^{-1} h^{-1}	H_2:CO_2:Ar = 80:20:30	0.295	65
Pd@Zn	45, 270	(W) 18000 mL g^{-1} h^{-1}	3	~0.60	47

[a] (G) = GHSV = volume flow rate/bed volume, (W) = WHSV = mass flow rate/catalyst mass.
[b] Space time yield of methanol ($g_{MeOH} \cdot g_{cat}^{-1} \cdot h^{-1}$)
[c] Microwave-assisted synthesis method

Conclusion

At comparable Cu loadings, catalyst derived from the ultra-thin AMO-LDH precursor $[(Cu_{0.47}Zn_{0.32}Ga_{0.21})(OH)_2](CO_3)_{0.105}\cdot m(H_2O)\cdot n(C_3H_6O)$ (LDH30Ga) was found to give higher Cu surface areas and better catalytic performance in terms of conversion, methanol selectivity and yield. It appears to be superior to the catalyst derived from LDH precursors with normal post-treatment (water wash) as well as the samples from conventional hydroxyl-carbonate precursors (CZG samples). Interestingly, this AMO-LDH precursor can maintain its ultra-thin layered morphology in spite of exhibiting an amorphous phase after calcination and can lead to accessible, well dispersed, small, and high surface area Cu crystallites decorated with a trace amount of Zn atoms. Moreover, this simple catalyst precursor not only displays a better space-time yield of methanol than the commercial HiFUEL^{TM} catalyst, but also outperforms those multi-doped LDHs as well as those recently-reported highly active catalysts in the literature. Overall, the current work presents the advantages of the AMOST method for preparing ultra-thin LDH catalyst precursors for CO_2 hydrogenation to methanol. According to our recent findings, the AMOST method can also be employed for preparing ultra-thin CuZnAl LDH system, however, this is beyond the scope of the current work. A more detailed study on other Cu-containing AMO-LDH systems including CuZnAl-LDH with the relevant ternary and quaternary LDH compositions will be published elsewhere. We believe, further optimization of AMO-LDH catalyst precursors can open new opportunities for the preparation of size-controlled small bimetallic nanocrystallites for many catalytic processes.

Supporting Information

Experimental description and supplementary experimental data.

Corresponding Author

* Corresponding author: edman.tsang@chem.ox.ac.uk

Author Contribution

M. M.-J. L. carried out synthesis, catalyst testing, data analysis and data interpretation; C. C. provided the initial AMO-LDH samples and advised on the synthesis and the structural investigation; T. A. and H. S. carried out some synthesis, testing, and thermogravimetric analysis. J. Z. performed N_2O chemisorption measurement; I. F. T. contributed for TEM images; Y. L. helped with SXRD measurement and analysis; H. Z. assisted in the catalyst testing; C. C. and H. S. were supervised by D. O. H.; S. C. E. T. supervised this project. M. M-J. L. and S. C. E. T. wrote the main manuscript text with the assistance of T.A. All authors discussed and reviewed this paper.

Conflict of Interest Disclosure

The authors declare no competing financial interest.

Acknowledgement

M. M.-J. L. acknowledges the Swire Scholarship of Oxford for her DPhil study.

REFERENCES

(1) Yu, K. M. K.; Curcic, I.; Gabriel, J.; Tsang, S. C. E. Recent Advances in CO_2 Capture and Utilization. *ChemSusChem* **2008**, *1*, 893–899.

(2) Turner, J.; Sverdrup, G.; Mann, M. K.; Maness, P.; Kroposki, B.; Ghirardi, M.; Evans, R. J.; Blake, D. Renewable Hydrogen Production. *Int. J. Energy Res.* **2008**, *32*, 379–407.

(3) Song, C. Global Challenges and Strategies for Control, Conversion and Utilization of CO_2 for Sustainable Development Involving Energy, Catalysis, Adsorption and Chemical Processing. *Catal. Today* **2006**, *115*, 2–32.

(4) Olah, G. A.; Goeppert, A.; Prakash, G. K. S. Beyond Oil and Gas: The Methanol Economy. *Angew. Chemie - Int. Ed.* **2005**, *44*, 2636–2639.

(5) Chinchen, G. C.; Waugh, K. C.; Whan, D. A. The Activity and State of the Copper Surface in Methanol Synthesis Catalysts. *Appl. Catal.* **1986**, *25*, 101–107.

(6) Burch, R.; Chappell, R. J. Support and Additive Effects in the Synthesis of Methanol over Copper Catalysts. *Appl. Catal.* **1988**, *45*, 131–150.

(7) Fujitani, T.; Nakamura, J. The Chemical Modification Seen in the Cu/ZnO Methanol Synthesis Catalysts. *Appl. Catal. A Gen.* **2000**, *191*, 111–129.

(8) Liao, F.; Zeng, Z.; Eley, C.; Lu, Q.; Hong, X.; Tsang, S. C. E. Electronic Modulation of a Copper/zinc Oxide Catalyst by a Heterojunction for Selective Hydrogenation of Carbon Dioxide to Methanol. *Angew. Chemie - Int. Ed.* **2012**, *51*, 5832–5836.

(9) Zander, S.; Kunkes, E. L.; Schuster, M. E.; Schumann, J.; Weinberg, G.; Teschner, D.; Jacobsen, N.; Schlögl, R.; Behrens, M. The Role of the Oxide Component in the Development of Copper Composite Catalysts for Methanol Synthesis. *Angew. Chemie - Int. Ed.* **2013**, *52*, 6536–6540.

(10) Spencer, M. S. The Role of Zinc Oxide in Cu/ZnO Catalysts for Methanol Synthesis and the Water-Gas Shift Reaction. *Top. Catal.* **1999**, *8*, 259–266.

(11) Fujitani, T.; Nakamura, J. The Effect of ZnO in Methanol Synthesis Catalysts on Cu Dispersion and the Specific Activity. *Catal. Letters* **1998**, *56*, 119–124.

(12) Kanai, Y.; Watanabe, T.; Fujitani, T.; Saito, M.; Nakamura, J.; Uchijima, T. Evidence for the Migration of ZnO_x in a Cu/ZnO Methanol Synthesis Catalyst. *Catal. Letters* **1994**, *27*, 67–78.

(13) Fujita, S., Usui, M., Ito, H., Takezawa, N. Mechanisms of Methanol Synthesis from Carbon Dioxide and from Carbon Monoxide at Atmospheric Pressure over Cu/ZnO. *J. Catal*. **1995**, *157*, 403–413.

(14) Choi, Y.; Futagami, K.; Fujitani, T.; Nakamura, J. Role of ZnO in Cu/ZnO Methanol Synthesis Catalysts - Morphology Effect or Active Site Model? *Appl. Catal. A Gen.* **2001**, *208*, 163–167.

(15) Hambrock, J.; Schröter, M. K.; Birkner, A.; Wöll, C.; Fischer, R. A. Nano-Brass: Bimetallic Copper/Zinc Colloids by a Nonaqueous Organometallic Route Using $[Cu(OCH(Me)CH_2NMe_2)_2]$ and Et_2Zn as Precursors. *Chem. Mater.* **2003**, *15*, 4217–4222.

(16) Sanches, S. G.; Flores, J. H.; De Avillez, R. R.; Pais Da Silva, M. I. Influence of Preparation Methods and Zr and Y Promoters on Cu/ZnO Catalysts Used for Methanol Steam Reforming. *Int. J. Hydrogen Energy* **2012**, *37*, 6572–6579.

(17) Derrouiche, S.; Lauron-Pernot, H.; Louis, C. Synthesis and Treatment Parameters for Controlling Metal Particle Size and Composition in Cu/ZnO Materials-First Evidence of Cu_3Zn Alloy Formation. *Chem. Mater.* **2012**, *24*, 2282–2291.

(18) Behrens, M.; Studt, F.; Kasatkin, I.; Kühl, S.; Hävecker, M.; Abild-pedersen, F.; Zander,

S.; Girgsdies, F.; Kurr, P.; Kniep, B.; Tovar, M.; Fischer, R. W.; Nørskov, J. K.; Schlögl, R. The Active Site of Methanol Synthesis over $Cu/ZnO/Al_2O_3$ Industrial Catalysts. *Science* **2012**, *336*, 893–898.

(19) Kattel, S.; Ramírez, P. J.; Chen, J. G.; Rodriguez, J. A.; Liu, P. Active Sites for CO_2 Hydrogenation to Methanol on Cu/ZnO Catalysts. *Science* **2017**, *355*, 1296–1299.

(20) Arena, F.; Barbera, K.; Italiano, G.; Bonura, G.; Spadaro, L.; Frusteri, F. Synthesis, Characterization and Activity Pattern of $Cu-ZnO/ZrO_2$ Catalysts in the Hydrogenation of Carbon Dioxide to Methanol. *J. Catal.* **2007**, *249*, 185–194.

(21) Saito, M.; Fujitani, T.; Takeuchi, M.; Watanabe, T. Development of Copper/zinc Oxide-Based Multicomponent Catalysts for Methanol Synthesis from Carbon Dioxide and Hydrogen. *Appl. Catal. A Gen.* **1996**, *138*, 311–318.

(22) Kurtz, M.; Wilmer, H.; Genger, T.; Hinrichsen, O.; Muhler, M. Deactivation of Supported Copper Catalysts for Methanol Synthesis. *Catal. Letters* **2003**, *86*, 77–80.

(23) An, X.; Li, J.; Zuo, Y.; Zhang, Q.; Wang, D.; Wang, J. A Cu/Zn/Al/Zr Fibrous Catalyst That Is an Improved CO_2 hydrogenation to Methanol Catalyst. *Catal. Letters* **2007**, *118*, 264–269.

(24) Weigel, J.; Koeppel, R. A.; Baiker, A.; Wokaun, A. Surface Species in CO and CO_2 Hydrogenation over Copper/zirconia: On the Methanol Synthesis Mechanism. *Langmuir* **1996**, *12*, 5319–5329.

(25) Yu, K. M. K.; Tong, W.; West, A.; Cheung, K.; Li, T.; Smith, G.; Guo, Y.; Tsang, S. C. E. Non-Syngas Direct Steam Reforming of Methanol to Hydrogen and Carbon Dioxide at Low Temperature. *Nat. Commun.* **2012**, *3*, 1230.

(26) Tong, W.; Cheung, K.; West, A.; Yu, K.-M.; Tsang, S. C. E. Direct Methanol Steam

Reforming to Hydrogen over $CuZnGaO_x$ Catalysts without CO Post-Treatment: Mechanistic Considerations. *Phys. Chem. Chem. Phys.* **2013**, *15*, 7240–7248.

(27) Tong, W.; West, A.; Cheung, K.; Yu, K. M.; Tsang, S. C. E. Dramatic Effects of Gallium Promotion on Methanol Steam Reforming Cu-ZnO Catalyst for Hydrogen Production: Formation of 5Å Copper Clusters from Cu-$ZnGaO_x$. *ACS Catal.* **2013**, *3*, 1231–1244.

(28) Schumann, J.; Eichelbaum, M.; Lunkenbein, T.; Thomas, N.; Álvarez Galván, M. C.; Schlögl, R.; Behrens, M. Promoting Strong Metal Support Interaction: Doping ZnO for Enhanced Activity of Cu/ZnO:M (M = Al, Ga, Mg) Catalysts. *ACS Catal.* **2015**, *5*, 3260–3270.

(29) Toyir, J.; Ramírez De La Piscina, P.; Fierro, J. L. G.; Homs, N. Highly Effective Conversion of CO_2 to Methanol over Supported and Promoted Copper-Based Catalysts: Influence of Support and Promoter. *Appl. Catal. B Environ.* **2001**, *29*, 207–215.

(30) Li, M. M.-J.; Zeng, Z.; Liao, F.; Hong, X.; Tsang, S. C. E. Enhanced CO_2 Hydrogenation to Methanol over CuZn Nanoalloy in Ga Modified Cu/ZnO Catalysts. *J. Catal.* **2016**, *343*, 157–167.

(31) Jiao, Y. N.; Hou, W. G. Effects of Structural Charges on Points of Zero Charge and Intrinsic Surface Reaction Equilibrium Constants of Zn-Al and Zn-Al-Fe Hydrotalcite-like Compounds. *Colloids Surf. A Physicochem. Eng. Asp.* **2007**, *296*, 62–66.

(32) Zhang, L.; Li, F.; Evans, D. G.; Duan, X. Structure and Surface Characteristics of Cu-Based Composite Metal Oxides Derived from Layered Double Hydroxides. *Mater. Chem. Phys.* **2004**, *87*, 402–410.

(33) Zhang, L. H.; Zheng, C.; Li, F.; Evans, D. G.; Duan, X. Copper-Containing Mixed Metal Oxides Derived from Layered Precursors: Control of Their Compositions and Catalytic

Properties. *J. Mater. Sci.* **2008**, *43*, 237–243.

(34) Behrens, M.; Kasatkin, I.; Kühl, S.; Weinberg, G. Phase-Pure Cu,Zn,Al Hydrotalcite-like Materials as Precursors for Copper Rich Cu/ZnO/Al_2O_3 Catalysts. *Chem. Mater.* **2010**, *22*, 386–397.

(35) Busca, G.; Costantino, U.; Marmottini, F.; Montanari, T.; Patrono, P.; Pinzari, F.; Ramis, G. Methanol Steam Reforming over Ex-Hydrotalcite Cu–Zn–Al Catalysts. *Appl. Catal. A Gen.* **2006**, *310*, 70–78.

(36) Chen, C.; Yang, M.; Wang, Q.; Buffet, J.-C.; O'Hare, D. Synthesis and Characterisation of Aqueous Miscible Organic-Layered Double Hydroxides. *J. Mater. Chem. A* **2014**, *2*, 15102–15110.

(37) Li, M. M. J.; Zheng, J.; Qu, J.; Liao, F.; Raine, E.; Kuo, W. C. H.; Su, S. S.; Po, P.; Yuan, Y.; Tsang, S. C. E. The Remarkable Activity and Stability of a Highly Dispersive Beta-Brass Cu-Zn Catalyst for the Production of Ethylene Glycol. *Sci. Rep.* **2016**, *6*, 4–11.

(38) Behrens, M.; Girgsdies, F.; Trunschke, A.; Schlögl, R. Minerals as Model Compounds for Cu/Zno Catalyst Precursors: Structural and Thermal Properties and IR Spectra of Mineral and Synthetic (Zincian) Malachite, Rosasite and Aurichalcite and a Catalyst Precursor Mixture. *Eur. J. Inorg. Chem.* **2009**, *2009*, 1347–1357.

(39) Baltes, C.; Vukojević, S.; Schüth, F. Correlations between Synthesis, Precursor, and Catalyst Structure and Activity of a Large Set of CuO/ZnO/Al_2O_3 Catalysts for Methanol Synthesis. *J. Catal.* **2008**, *258*, 334–344.

(40) Behrens, M. Meso- and Nano-Structuring of Industrial Cu/ZnO/(Al_2O_3) Catalysts. *J. Catal.* **2009**, *267*, 24–29.

(41) Gao, P.; Zhong, L.; Zhang, L.; Wang, H.; Zhao, N.; Wei, W.; Sun, Y. Yttrium Oxide

Modified $Cu/ZnO/Al_2O_3$ Catalysts via Hydrotalcite-like Precursors for CO_2 Hydrogenation to Methanol. *Catal. Sci. Technol.* **2015**, *5*, 4365–4377.

(42) Cheng, J.; Wang, X.; Yu, J.; Hao, Z.; Xu, Z. P. Sulfur-Resistant NO Decomposition Catalysts Derived from Co-Ca/Ti-Al Hydrotalcite-like Compounds. *J. Phys. Chem. C* **2011**, *115*, 6651–6660.

(43) Wang, Q.; O'Hare, D. Recent Advances in the Synthesis and Application of Layered Double Hydroxide (LDH) Nanosheets. *Chem. Rev.* **2012**, *112*, 4124–4155.

(44) Fichtl, M. B.; Schumann, J.; Kasatkin, I.; Jacobsen, N.; Behrens, M.; Schlögl, R.; Muhler, M.; Hinrichsen, O. Counting of Oxygen Defects versus Metal Surface Sites in Methanol Synthesis Catalysts by Different Probe Molecules. *Angew. Chemie - Int. Ed.* **2014**, *53*, 7043–7047.

(45) Kuld, S.; Conradsen, C.; Moses, P. G.; Chorkendorff, I.; Sehested, J. Quantification of Zinc Atoms in a Surface Alloy on Copper in an Industrial-Type Methanol Synthesis Catalyst. *Angew. Chemie - Int. Ed.* **2014**, *53*, 5941–5945.

(46) Kuld, S.; Thorhauge, M.; Falsig, H.; Elkjaer, C. F.; Helveg, S.; Chorkendorff, I.; Sehested, J. Quantifying the Promotion of Cu Catalysts by ZnO for Methanol Synthesis. *Science* **2016**, *352*, 969–974.

(47) Liao, F.; Wu, X.-P.; Zheng, J.; Li, M. M.-J.; Kroner, A.; Zeng, Z.; Hong, X.; Yuan, Y.; Gong, X.-Q.; Tsang, S. C. E. A Promising Low Pressure Methanol Synthesis Route from CO_2 Hydrogenation over Pd@Zn Core–shell Catalysts. *Green Chem.* **2017**, *19*, 270–280.

(48) Fujitani, T.; Saito, M.; Kanai, Y.; Watanabe, T.; Nakamura, J.; Uchijima, T. Development of an Active Ga_2O_3 Supported Palladium Catalyst for the Synthesis of Methanol from Carbon Dioxide and Hydrogen. *Appl. Catal. A Gen.* **1995**, *125*, 199–202.

(49) Gao, P.; Zhong, L.; Zhang, L.; Wang, H.; Zhao, N.; Wei, W.; Sun, Y. Yttrium Oxide Modified $Cu/ZnO/Al_2O_3$ Catalysts via Hydrotalcite-like Precursors for CO_2 Hydrogenation to Methanol. *Catal. Sci. Technol.* **2015**, *5*, 4365–4377.

(50) Xiao, S.; Zhang, Y.; Gao, P.; Zhong, L.; Li, X.; Zhang, Z.; Wang, H.; Wei, W.; Sun, Y. Highly Efficient Cu-Based Catalysts via Hydrotalcite-like Precursors for CO_2 hydrogenation to Methanol. *Catal. Today* **2017**, *281*, 327–336.

(51) Van Den Berg, R.; Prieto, G.; Korpershoek, G.; Van Der Wal, L. I.; Van Bunningen, A. J.; Lægsgaard-Jørgensen, S.; De Jongh, P. E.; De Jong, K. P. Structure Sensitivity of Cu and CuZn Catalysts Relevant to Industrial Methanol Synthesis. *Nat. Commun.* **2016**, *7*, 13057.

(52) Behrens, M. Chemical Hydrogen Storage by Methanol: Challenges for the Catalytic Methanol Synthesis from CO_2. *Recycl. Catal.* **2015**, *2*, 78–86.

(53) Van Helden, P.; Ciobîcə, I. M.; Coetzer, R. L. J. The Size-Dependent Site Composition of FCC Cobalt Nanocrystals. *Catal. Today* **2016**, *261*, 48–59.

(54) Moudler, J. F.; Stickle, W. F.; Sobol, P. E.; Bomben, K. D. *Handbook of X-Ray Photoelectron Spectroscopy: A Reference Book of Standard Spectra for Identification and Interpretation of XPS Data*; Physical Electronics Division, Perkin-Elmer Corporation, Eden Prairie, 1992.

(55) Günter, M. M.; Ressler, T.; Bems, B.; Büscher, C.; Genger, T.; Hinrichsen, O.; Muhler, M.; Schlögl, R. Implication of the Microstructure of Binary Cu/ZnO Catalysts for Their Catalytic Activity in Methanol Synthesis. *Catal. Letters* **2001**, *71*, 37–44.

(56) Burch, R.; Golunski, S. E.; Spencer, M. S. The Role of Copper and Zinc Oxide in Methanol Synthesis Catalysts. *J. Chem. Soc. Faraday Trans.* **1990**, *86*, 2683–2691.

(57) Klier, K. Methanol Synthesis. *Adv. Catal.* **1982**, *31*, 243–313.

(58) Frost, J. C. Junction Effect Interactions in Methanol Synthesis Catalysts. *Nature* **1988**, *334*, 577–580.

(59) Hansen, P. L.; Wagner, J. B.; Helveg, S.; Rostrup-Nielsen, J. R.; Clausen, B. S.; Topsøe, H. Atom-Resolved Imaging of Dynamic Shape Changes in Supported Copper Nanocrystals. *Science* **2002**, *295*, 2053–2055.

(60) Gao, P.; Li, F.; Xiao, F.; Zhao, N.; Wei, W.; Zhong, L.; Sun, Y. Effect of Hydrotalcite-Containing Precursors on the Performance of Cu/Zn/Al/Zr Catalysts for CO_2 Hydrogenation: Introduction of Cu^{2+} at Different Formation Stages of Precursors. *Catal. Today* **2012**, *194*, 9–15.

(61) Gao, P.; Li, F.; Zhao, N.; Xiao, F.; Wei, W.; Zhong, L.; Sun, Y. Influence of Modifier (Mn, La, Ce, Zr and Y) on the Performance of Cu/Zn/Al Catalysts via Hydrotalcite-like Precursors for CO_2 Hydrogenation to Methanol. *Appl. Catal. A Gen.* **2013**, *468*, 442–452.

(62) Kühl, S.; Schumann, J.; Kasatkin, I.; Hävecker, M.; Schlögl, R.; Behrens, M. Ternary and Quaternary Cr or Ga-Containing Ex-LDH Catalysts - Influence of the Additional Oxides onto the Microstructure and Activity of $Cu/ZnAl_2O_4$ catalysts. *Catal. Today* **2015**, *246*, 92–100.

(63) Cai, W.; De La Piscina, P. R.; Toyir, J.; Homs, N. CO_2 Hydrogenation to Methanol over CuZnGa Catalysts Prepared Using Microwave-Assisted Methods. *Catal. Today* **2015**, *242*, 193–199.

(64) Saito, M. R&D Activities in Japan on Methanol Synthesis from CO_2 and H_2. *Catal. Surv. From Japan* **1998**, *2*, 175–184.

(65) Martin, O.; Martin, A. J.; Mondelli, C.; Mitchell, S.; Segawa, T. F.; Hauert, R.; Drouilly, C.; Curulla-Ferré, D.; Pérez-Ramírez, J. Indium Oxide as a Superior Catalyst for Methanol

Synthesis by CO_2 Hydrogenation. *Angew. Chemie - Int. Ed.* **2016**, *55*, 6261–6265.

(66) Liao, F.; Wu, X.-P.; Zheng, J.; Li, M.-J.; Zeng, Z.; Hong, X.; Kroner, A.; Yuan, Y.; Gong, X.-Q.; Tsang, S. C. E. Pd@Zn Core–shell Nanoparticles of Controllable Shell Thickness for Catalytic Methanol Production. *Catal. Sci. Technol.* **2016**, *6*, 7698–7702.

(67) Kühl, S.; Tarasov, A.; Zander, S.; Kasatkin, I.; Behrens, M. Cu-Based Catalyst Resulting from a Cu,Zn,Al Hydrotalcite-like Compound: A Microstructural, Thermoanalytical, and in Situ XAS Study. *Chem. - A Eur. J.* **2014**, *20*, 3782–3792.

(68) Wang, J.; Li, G.; Li, Z.; Tang, C.; Feng, Z.; An, H.; Liu, H.; Liu, T.; Li, C. A Highly Selective and Stable ZnO-ZrO_2 Solid Solution Catalyst for CO_2 Hydrogenation to Methanol. *Sci. Adv.* **2017**, *3*, e1701290.

Table of Contents Graphic: